Second Quarterly Report
for

# SOLAR CELL COVER GLASS DEVELOPMENT

( 1 September 1966 through 30 November 1966 )

Contract Number: NAS5-10236

Prepared by:

Ion Physics Corporation
Burlington, Massachusetts

Prepared for:

Goddard Space Flight Center
Greenbelt, Maryland



ION PHYSICS CORPORATION IPC

A Subsidiary of High Voltage Engineering Corporation

BURLINGTON, MASSACHUSETTS

Quarterly Technical Progress Report No. 2

1 September 1966 through 30 November 1966

# SOLAR CELL COVER GLASS DEVELOPMENT

National Aeronautics and Space Administration
Goddard Space Flight Center
Greenbelt, Maryland

Contract NAS5-10236


Project Manager: Dr. William J. King

Project Engineer: Stanley J. Solomon



ION PHYSICS CORPORATION
BURLINGTON, MASSACHUSETTS

## CONFERENCES

A conference was held at Ion Physics Corporation on 2 November 1966 at which Mr. W. Cherry discussed program accomplishments with IPC personnel.

# OBJECTIVE

The objective of this program is refinement and economic optimization of techniques for fabrication of thick integral coverslips for silicon solar cells. An a priori assumption is that integral coverslip cells must show a definite superiority over conventional glued coverslip cells. The consequences of this assumption provide natural guidelines for selection of candidate coverslip materials, possible fabrication techniques and environmental test end points. Specifically, all coverslip materials that are known to significantly degrade under ultra violet, proton or electron irradiation must be categorically excluded from consideration. Similarly, all fabrication techniques that are inherently deleterious to the cell structure itself must be rejected. Finally, the environmental and radiation test end points must be at least as severe as those encountered with glued coverslip cells. For ease in comparison, final testing is to be done on cells with 6 mil integral coverslips.

## SUMMARY

IPC's proprietary high vacuum sputtering process has been shown to be well suited to the deposition of integral $SiO_2$ coverslips onto silicon solar cells. Since, however, this process has a rate limitation, it is important to examine other processes that could more quickly deposit $SiO_2$ over an initial high vacuum sputtered layer. Both reactive sputtering and electron beam evaporation have been investigated as a means of building up coverslip thickness.

Neither of these processes is presently capable of depositing satisfactory thick layers of $SiO_2$. The reactively sputtered $SiO_2$ layers are hard and well bonded but contain many optical scattering centers when thick films are produced. The scattering centers appear to be related to the manner in which the Si cathode is supported. This problem is not presently solved. Electron beam evaporated $SiO_2$ is also well bonded but is soft and "frothy". This type of physical structure has been observed on all thick electron beam evaporated $SiO_2$, produced by both IPC and outside vendors, and may be inherent in $SiO_2$ evaporation. Although Temescal Metallurgical Corporation claims to be able to evaporate thick $SiO_2$ with an acceptable homogeneous structure, this has not yet been fully substantiated by IPC. While all evaporated $SiO_2$ has been of poor quality, a very pronounced effect of substrate temperature has been observed. Thick $SiO_2$ films deposited at ~ 20°C have shattered the Si substrate within eight hours after removal from the chamber. Thick films deposited at ~ 100°C have shown extremely poor structure, while films deposited below room temperature have stripped.

Integral coverslipped solar cells shipped to NASA with the First Quarterly Report withstood rapid temperature cycling between -196 and + 100°C. Cells with up to 3 mil of high vacuum sputtered $SiO_2$ were tested. Cells with 4 mils of high vacuum sputtered $SiO_2$ have been produced during this quarter. These cells have also been rapidly temperature cycled between -196 and + 100°C. Cells with 2 mil $SiO_2$ integral coverslips have been stored in a vacuum of $\sim 2 \times 10^{-7}$ torr for 500 hours at 100°C with no detectable loss in weight. Other cells, with 2 mil $SiO_2$ integral coverslips, have been irradiated with 0.4 Mev protons at fluxes of $10^{13}$, $10^{14}$ and $10^{15}$ protons-cm$^{-2}$ with no measurable degradation.

TABLE OF CONTENTS


| | | Page |
|---|---|---|
| | CONFERENCES | iii |
| | OBJECTIVE | iv |
| | SUMMARY | v |
| 1. | PROGRAM CONSIDERATIONS | 1 |
| | 1.1 Integral Coverslips | 1 |
| | 1.1.1 Micrometeorite Protection | 1 |
| | 1.1.2 Radiation Protection | 3 |
| | 1.2 Radiation Damage | 9 |
| | 1.2.1 Fused Silica | 9 |
| | 1.2.2 Aluminum Oxide | 9 |
| | 1.2.3 Other Materials | 10 |
| 2. | EXPERIMENTAL RESULTS | 11 |
| | 2.1 Deposition Techniques | 11 |
| | 2.1.1 High Vacuum Sputtering | 12 |
| | 2.1.2 Electron Beam Evaporation | 16 |
| | 2.1.3 Reactive Sputtering | 21 |
| | 2.2 Cell Testing | 27 |
| | 2.2.1 Vacuum Environment | 27 |
| | 2.2.2 Proton Resistance | 27 |
| 3. | FUTURE PLANS | 31 |
| 4. | REFERENCES | 33 |

LIST OF ILLUSTRATIONS


| Figure | | Page |
|---|---|---|
| 1 | Degradation of Diffusion Length in 1 ohm-cm p-Type Silicon as a Function of Integrated Electron Flux | 4 |
| 2 | Typical Spectral Response of 1 ohm-cm n/p Solar Cell to 1.0 Mev Electrons | 5 |
| 3 | Range-Energy Relationship for Protons in $SiO_2$ | 7 |
| 4 | Range-Energy Relationship for Electrons in Aluminum | 8 |
| 5 | High Current High Vacuum Sputtering System Schematic | 14 |
| 6 | High Current High Vacuum Sputtering System | 15 |
| 7 | High Vacuum Sputtering-Electron Beam Evaporation Apparatus | 17 |
| 8 | Installed Electron Gun | 18 |
| 9 | First Reactive Sputtering System | 22 |
| 10 | Second Reactive Sputtering System | 23 |
| 11 | Third Reactive Sputtering Configuration | 24 |
| 12 | Sixth Reactive Sputtering System | 26 |

# LIST OF TABLES


| Table | | Page |
|---|---|---|
| 1 | Hardness of Candidate Coverslip Materials | 2 |
| 2 | Vacuum Storage at 100°C | 28 |
| 3 | First Proton Test | 28 |
| 4 | Second Proton Test | 28 |
| 5 | Third Proton Test | 29 |

# 1. PROGRAM CONSIDERATIONS

## 1.1 Integral Coverslips

Solar cell coverslips have two distinct functions. The first, and least important, is protection of the cell from micrometeorite erosion. The second is protection of the cell from proton and (to some extent) electron bombardment damage.

### 1.1.1 Micrometeorite Protection

While micrometeorite fluxes and distributions are highly variable, they are now know to be far less of a solar cell hazard than had once been expected. The action of impacting micrometeorites or "space dust" on an unslipped cell is erosion and chipping of the top cell surface. In addition to removing the anti-reflection coating, this action produces further reductions in cell conversion efficiency by increasing the sheet resistance of the front layer and, in later stages, by eroding away significant fractions of the front, blue-responsive layer itself. Because the Ti-Ag contact fingers are relatively soft, as compared to silicon, damage rates on the fingers are much lower than on the cell surface.

While any coverslip would prevent cell surface erosion, an ideal slip should be very hard and should be applied without voids at the cell-slip interface. The latter requirement, also necessary to reduce interface reflection losses, is introduced to insure that relatively heavy dust particles cannot punch a hole in the slip by impacting on unsupported areas. The erosion resistance of the slip increases with its hardness. (Soft materials, like rubbers and soft metals, also have high erosion resistance but are not sufficiently transparent.) Table 1 lists hardnesses of candidate coverslip materials. All except the Knoop value for $Si_3N_4$ are from measurements on bulk materials and may be slightly different in film form. In any case, it can be seen that $Si_3N_4$ and $Al_2O_3$ are far more abrasion resistant than other candidate materials with $SiO_2$ being a poor third choice. While the use of $Si_3N_4$ coverslips has not been established as practical, $Al_2O_3$ certainly is an acceptable material. Thus, $Al_2O_3$ would, from this standpoint, be a better coverslip material than $SiO_2$.

One final point concerns reflections and scattering losses than would occur as a result of micrometeorite action on the coverslips themselves. While it is obvious that the anti-reflection coating on the outer surface of the slip would be lost first, resulting in an $\sim 2\%$ drop in conversion efficiency, further erosion would cause faceting of the slip surface. Since all candidate coverslip materials possess refractive indices higher than that of vacuum ($n \equiv 1.0$), the surface facets will cause multiple reflection and scattering of the incident light. Scattering does not, however, significantly reduce the intensity of the transmitted light. Thus conversion efficiency losses due to surface faceting would be much smaller than losses incurred through erosion of the anti-reflection

Table 1. Hardness of Candidate Coverslip Materials

| Material | Hardness[1] Knoop | Mohs |
|---|---|---|
| MgO | 370 | - |
| $SiO_2$ | 820 | 7 |
| $Al_2O_3$ | 2100 | 9+ |
| $Si_3N_4$ | 4000[2] | 9+ |

(1) "Handbook of Chemistry and Physics", 46th Edition, Chemical Rubber Company, Cleveland, Ohio (1965), p. F-15.

(2) K. E. Bean, P. S. Gleim, and W. R. Runyan, Abstract No. 147, Presented at October 1966 Electrochemical Society Meeting (Philadelphia).

layer. In the unlikely event that a slipped cell encounters significant micrometeorite densities the maximum conversion efficiency loss would be ~ 2%.

### 1.1.2 Radiation Protection

Energetic nuclear radiation incident on a semiconductor produces instantaneous electrical effects and permanent radiation damage. The damage consists of isolated or clustered lattice vacancies, interstitial atoms in a 1 to 1 correspondence (Frenkel defects) with the vacancies and, in some cases, interstitial atoms of the incident species. Physically this lattice disorder gives rise, at moderate dosage, to trapping levels that decrease the minority carrier lifetime. Figure 1 displays a typical result for proton irradiated p-type silicon. In solar cells, the decreased lifetime produces a serious degradation in conversion efficiency through loss of current from hole-electron pairs generated far from the junction by less strongly absorbed (red) light. Figure 2 displays a typical result for electron irradiated n/p cells. While higher radiation dosages produce further deleterious effects in semiconductors, solar cells are rendered useless by these moderate dosages.

In order to protect solar cells from radiation effects, it is first necessary to determine what type of protection is required. The capsular result of a multitude of space measurements is that for near-earth missions, one need be concerned only with electron and proton fluxes in the two Van Allen belts and solar flare protons. For deep space missions, solar flare protons only need be considered. These conclusions are based on the observation that fluxes of other particles or the same particles in other regions of space are relatively small and often of sufficient energy as to make cell shielding completely impractical. Since data on the flux and energy distribution of belt protons and electrons is readily available elsewhere, it is sufficient to note that the outer belt is predominantly an electron belt while the inner belt is predominantly a proton belt. While both high and low energy protons and electrons are involved, it will be shown below that it is only practical to shield against low energy proton damage.

Proton absorption proceeds through energy dependent compound mechanisma that involve both electronic excitation and elastic nuclear scattering. The former is active in the initial part of the proton range while the latter mechanism is important only at range end. (With very high energy protons, other scattering mechanisms also become important. They will not be discussed since these protons occur in space at low densities and cannot be effectively shielded.)

Elastic nuclear scattering produces lattice displacements (vacancy-interstitial pairs) and interstitial bombarding atoms. These, in turn, reduce minority carrier lifetime. Electronic excitation contributes to transient electrical phenomena but produces no permanent damage except in the case that electrons ionized from a lattice atom are given an energy in excess of 250 kev

Reproduced from: Rosenzweig, W., "Radiation Damage Studies", Presented at the IEEE Photovoltaic Specialists Meeting, Washington (April 1963).

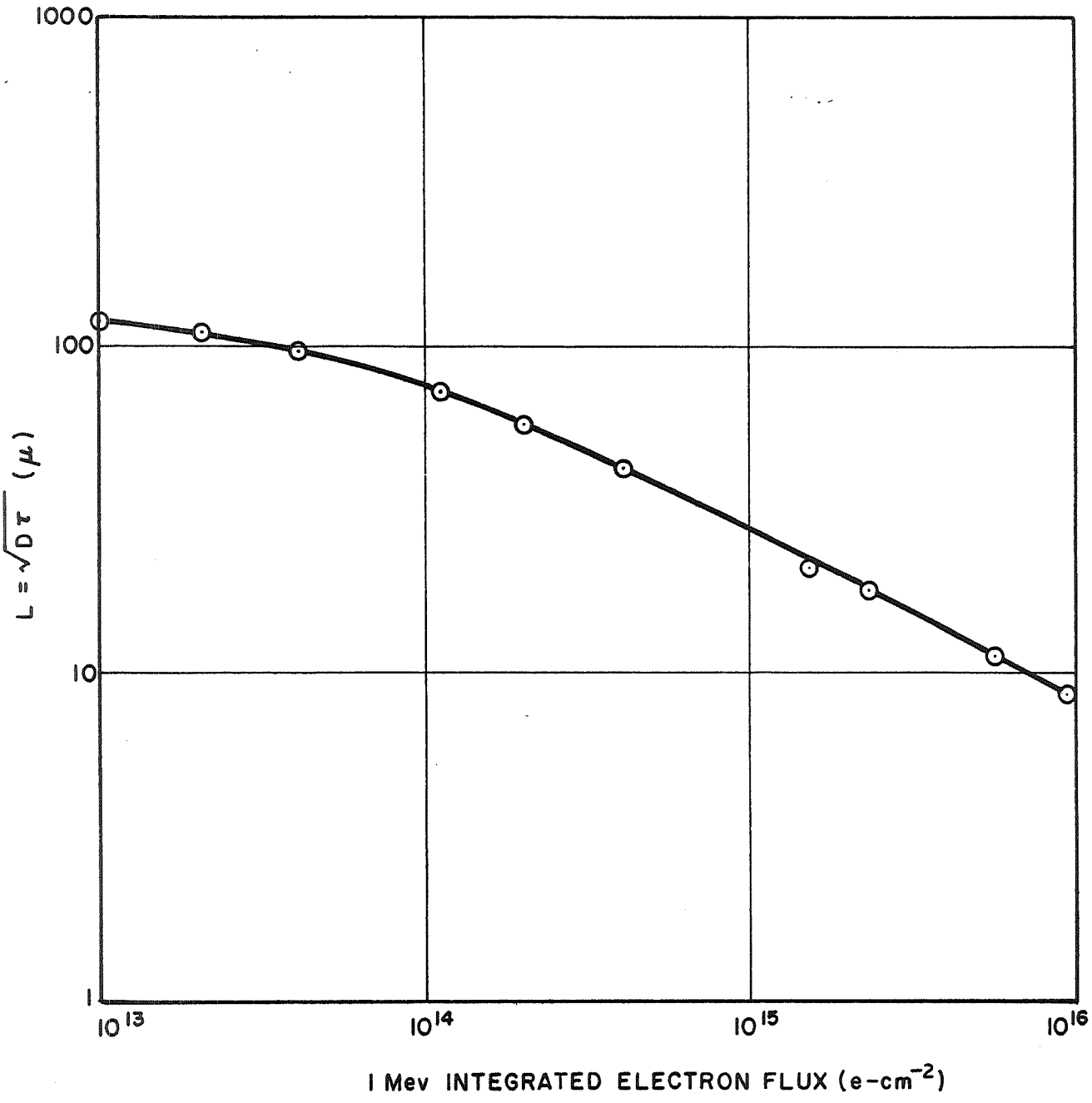


Figure 1. Degradation of Diffusion Length in 1 ohm-cm p-Type Silicon as a Function of Integrated Electron Flux

1-1916

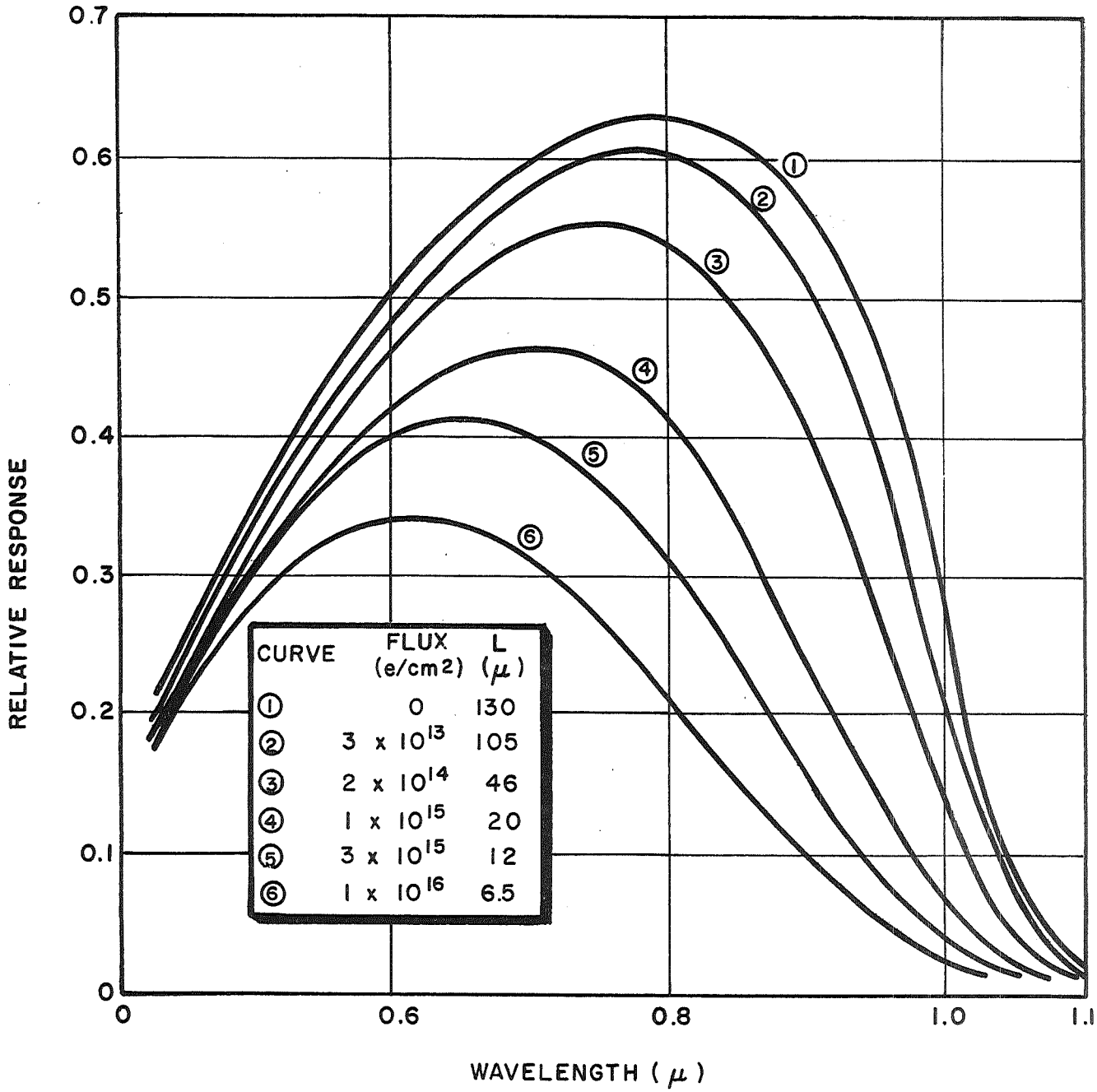


Reproduced from: Cooley, W. C. and Janda, R. J., "Handbook of Space-Radiation Effects on Solar-Cell Power Systems", NASA SP-3003 (1963).

Figure 2. Typical Spectral Response of 1 ohm-cm n/p Solar Cells to 1.0 Mev Electrons

1-1917

in a collision between a proton and lattice atom. In this case, the ionized electron is sufficiently energetic to cause lattice displacements in a collision.

These proton stopping mechanisms result in the path of a proton in a solid being describable by a mean range with a Gaussian distribution of end points about this mean. For low proton energies, the width of the distribution is about the same as the mean range. As the proton energy increases, the percentage width of the distribution decreases. The entire problem of proton range-energy relations has been fully discussed in Air Force Weapons Laboratory Publication AFWL-TR-65-150.[1] Unfortunately, these calculations have not been performed for any of the candidate coverslip materials. As a consequence, good range-energy data is only available for $SiO_2$.[2] This data is summarized in Figure 3. From this data it can be seen that a 6 mil coverslip will stop a 5 Mev proton while a 20 mil coverslip is required to stop an 8.5 Mev proton. Since these ranges are only mean values and the distribution is actually Gaussian, the high range components of the distribution may still penetrate to the cell surface. A 6 mil slip is therefore only adequate to stop all protons of energy ~ 3 Mev and a 20 mil slip will stop only 6 Mev protons.

Electron energy loss is due to the inelastic collisions of the electrons with the atomic electrons, by which the atoms are excited or ionized, and to the emission of bremsstrahlung in the coulomb field of the nucleus. The important consideration for these purposes is that electrons lose a large fraction of their energy in a single collision and hence are scattered out of the incident beam. As a result, the incident electron intensity is exponentially reduced in its passage through matter. The rate of intensity decrease is proportional to an absorption coefficient which is characteristic of the particular material for a given range of electron energies.

Incident electrons with energies < 250 kev produce only transient electrical effects in a solar cell. Electrons with energies > 250 kev can produce vacancy-interstitial pairs that degrade minority carrier lifetime. Again the best available electron range data for $SiO_2$ is in the Linnenbom paper.[2] This data is summarized in Figure 4, which is a plot of the range-energy curve for aluminum. The range in $SiO_2$ is 96% of the aluminum range. Thus a 6 mil coverslip will stop 170 kev electrons, while a 20 mil coverslip will stop only 380 kev electrons.

Since the weight of a typical 1 x 2 cm cell is ~ 12 mg/mil of cell thickness and the weight of a 1 x 2 cm $SiO_2$ coverslip is ~ 11 mg/mil of slip, it is readily seen that shielding against electrons and high energy protons can only be accomplished by a large sacrifice in power-to-weight ratio.

Reproduced from: Linnenbom, V. J., "Range-Energy Relations for Protons and Electrons in Al, Si and $SiO_2$", NRL Report 5828 (1962).

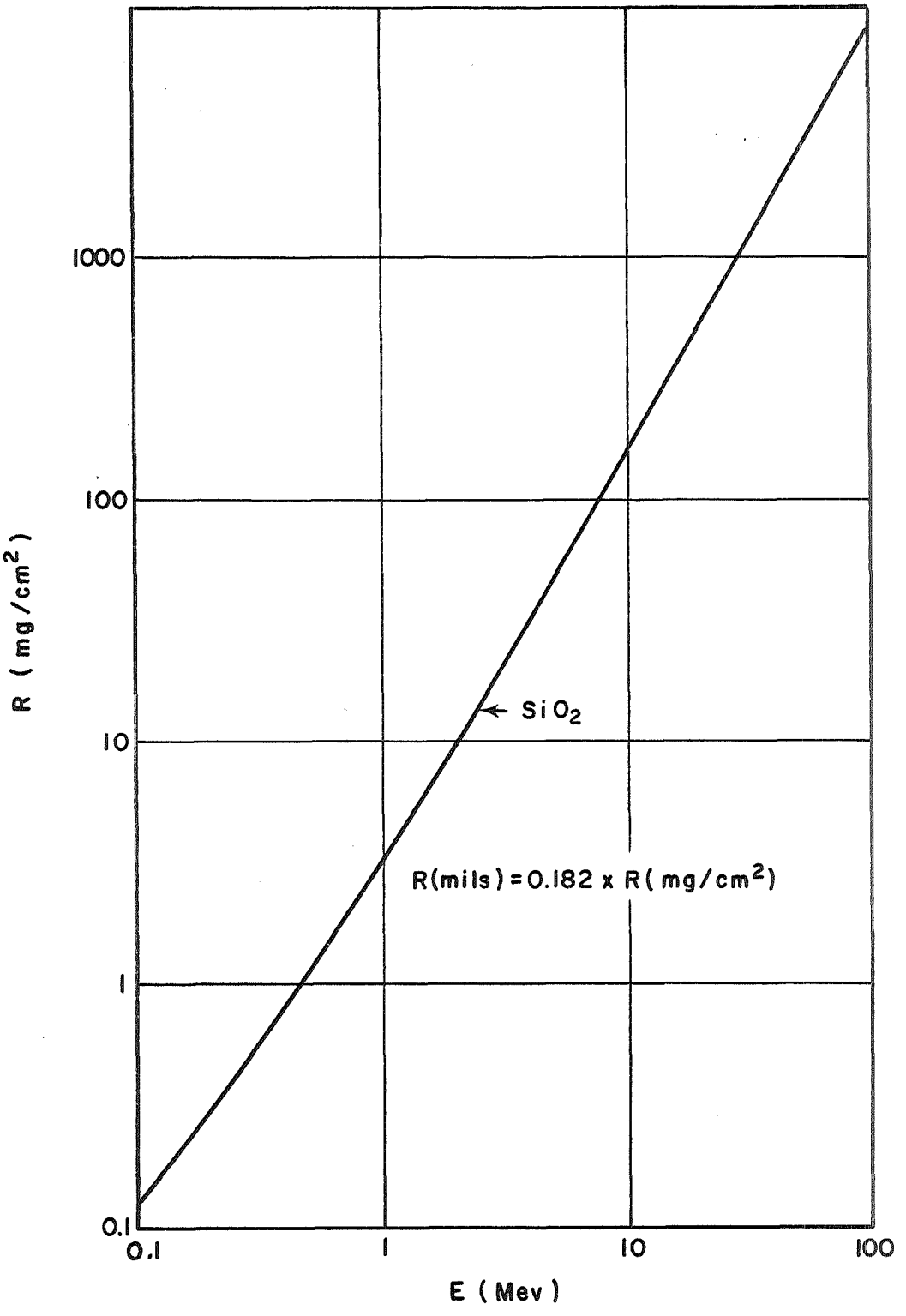


1-1918 Figure 3. Range-Energy Relationship for Protons in $SiO_2$

Reproduced from: Linnenbom, V. J., "Range-Energy Relations for Protons and Electrons in Al, Si and $SiO_2$", NRL Report 5828 (1962).

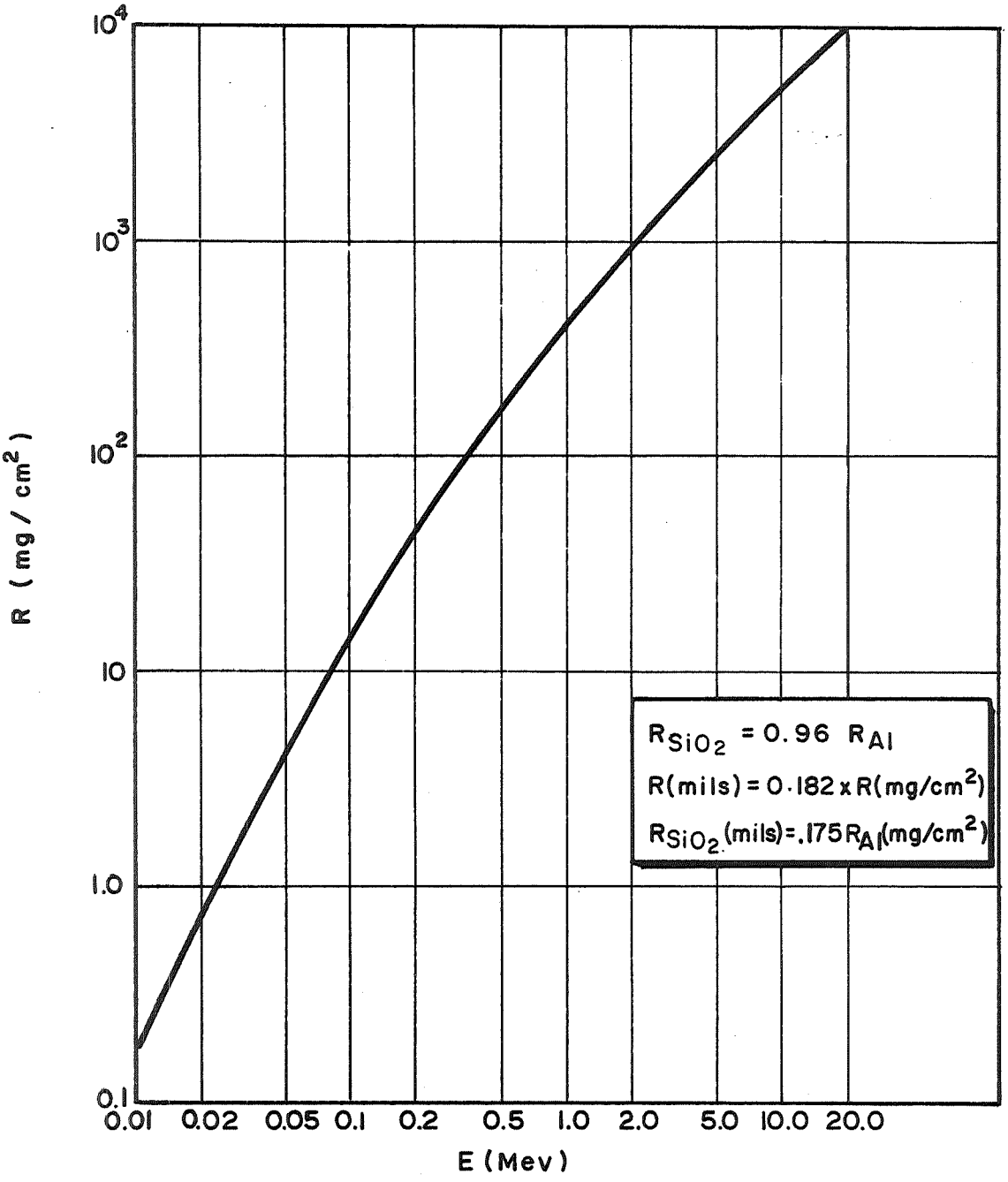


Figure 4. Range-Energy Relationship for Electrons in Aluminum

1-1919

## 1.2 Radiation Damage

This section is restricted to an examination of radiation damage in candidate coverslip materials. Damage effects in both solar cells themselves and in adhesives used to attach conventional coverslips have been fully discussed in the literature. As noted in the preceding section, only damage due to protons and electrons need be considered.

While all candidate coverslip materials are transparent amorphous dielectrics, short range lattice order is present. This allows amorphous structures to be discussed in terms of local crystalline structure.

### 1.2.1 Fused Silica

The marked optical transmission differences between fused quartz and fused silica after exposure to high electron fluxes (see Table IV of First Quarterly Report) are thought to be indicative of impurity effects. Products known as "fused quartz" are prepared from sand or crushed crystal quartz while those known as "fused silica" are prepared from synthetic $SiO_2$ powder. Electron darkening results indicate the latter product is much purer.

Radiation effects in crystalline and amorphous $SiO_2$ have been the subject of extensive investigation. Unfortunately, for the present purposes, most of these investigations have dealt with neutron damage. Neutron damage may be taken as a "worst case" of proton or electron damage since the former produces agglomerated spikes of lattice displacement, while the latter produce only relatively isolated displacements. On the other hand, cognizance must be taken of the charge of protons and electrons, because ionization effects are also possible in $SiO_2$. These studies are well summarized in Chapter 7 of Billington and Crawford[3] and in a chapter of International School of Physics, "Radiation Damage in Solids".[4]

The general conclusions of these studies is that aluminum impurities are responsible for radiation darkening in $SiO_2$. In high purity fused silica there is no appreciable darkening except for a weak OH absorption band in the IR. Since integral coverslips are deposited from either fused silica or silicon, the resultant coverslips would be expected to be as resistant to radiation darkening as fused silica. Completed tests on proton damage confirm this.

### 1.2.2 Aluminum Oxide

For the present purposes, pure $Al_2O_3$ may be considered as being extremely resistant to radiation darkening. This generalization is based on observations that $Al_2O_3$ (sapphire) does not darken under $10^{17}$ electron-$cm^{-2}$ at 1.2 Mev (see Table IV of First Quarterly Report) and that X-ray and neutron coloration is very small and, except for a weak gamma-produced peak at

4000 Å, confined to the region below 3000 Å. Chapter 8 of Billington and Crawford[5] gives a fuller discussion of $Al_2O_3$ darkening.

While most of the radiation darkening work in $Al_2O_3$ has been done with sapphire (single crystal $Al_2O_3$), it is though that coloration is not associated with lattice effects, in this case. Consequently, amorphous $Al_2O_3$ coverslips deposited in this program would be expected to show resistance to radiation darkening equivalent to that of sapphire.

### 1.2.3 Other Materials

MgO has also been well studied and the causes of coloration have been assigned. Of the many absorption bands observed, all occur below 3250 Å except for a band at 5200 Å that is produced by all types of radiation.[6] The stability of all these bands is dependent on the type of radiation used and is great only for neutron-produced coloration. These bands are thought to be due to radiation produced valence changes in a transition metal impurity present in commercial quality MgO. This suggests that starting materials (Mg or MgO) need only be carefully selected for purity.

Radiation darkening studies with lead glasses have been done on an engineering basis rather than on a scientific basis. High flux levels do produce slight darkening in the visible region. Since these glasses were formulated to resist radiation darkening, little improvement could be expected.

While $Si_3N_4$ is at present a very popular material, IPC is unaware of any studies of its radiation darkening behavior.

# 2. EXPERIMENTAL RESULTS

## 2.1 Deposition Techniques

An extensive number of techniques for growing or depositing $SiO_2$ on silicon have been reported. Other than vacuum evaporation, sputtering and plasma techniques, all these processes require at least one operation in the range of 450 to 1200°C. Since integral coverslips must be applied to a completed solar cell, thermal cycles in the high temperature end of this range must be categorically excluded. Depending on the total "quality" of the cell contacts, thermal operations at temperatures up to 550°C can be tolerated although they certainly are undesirable. Unfortunately, those thermal processes that operate is this narrow acceptable temperature range do not produce pure $SiO_2$ coatings but rather $SiO_2$ contaminated with hydrocarbon fragments. As there is little reason to expect these fragments to be optically stable with respect to space vacuum and radiation environments, these few processes must also be rejected. It should be noted that in all of the above processes, films thicker than 10 to 20 x $10^3$ Å spontaneously strip from the silicon substrate. This is presumably due to a combination of thermal mismatch between silicon and $SiO_2$ and the high processing temperatures producing sufficient strain to shear the $Si\text{-}SiO_2$ interface.

Of the three remaining techniques, only vacuum evaporation has been fully explored. Here again, film thicker than 10 to 20 x $10^3$ Å spontaneously strip from silicon. In this case, however, deposition occurs reasonably near room temperature so that large thermal excursions are not involved. The spontaneous stripping must then be due to intrinsic strain in the deposited layer and/or the inherently poor bonding of evaporated films.

Plasma techniques, relatively recent developments, take one of two forms. In the first form, electrical energy is substituted for thermal energy in dissociating $O_2$ to allow growth of $SiO_2$ at lower temperatures. While this technique appears quite effective, it is basically an oxide growth technique and operates by diffusion of the oxidant through the existing oxide to the $Si\text{-}SiO_2$ interface. This leads to something approaching the parabolic film growth rate dependence obtained from conventional high temperature oxidation and the limiting case of ~ 15 x $10^3$ Å $SiO_2$ films in practical times.

In the second form, the plasma is used to dissociate a silicon organo-metallic. This technique, a variation on a more general deposition process that has been under investigation at IPC since 1961, deposits good quality $SiO_2$ on room temperature substrates but only at rates of 6 to 10 x $10^3$ Å-$hr^{-1}$.

By elimination then, only sputtering techniques remain. Glow discharge and triode sputtering are not applicable to sputtering $SiO_2$ since these processes can only be used with conducting cathodes. While RF sputtering of

$SiO_2$ is applicable, equipment for producing 1 mil coverslips on 5000 1 x 2 cm cells per week has been quoted at $200,000. (More recent information suggests these capital costs could be lowered.) On the other hand, reactive sputtering of Si in an Ar-$O_2$ mixture appeared both practical and economic. While IPC demonstrated initial feasibility of this approach in early 1966, thick $SiO_2$ films again stripped from silicon.

IPC, during the past four years, has developed a technique for sputtering in high vacuum, that is an improvement upon conventional sputtering. Films of $SiO_2$, greater than 1 mil thick, deposited on completed solar cells were shown to be stable with respect to thermal cycling (77 to 480°K) and to be unaffected by proton bombardment up to $10^{15}$ -$cm^{-2}$. While the IPC high vacuum sputtering process is uniquely capable of depositing $SiO_2$ integral coverslips that satisfy the contract requirements, the deposition rates that can be economically achieved are lower than would be desired for production of multiple mil thick coverslips. One objective of this program is to determine if either reactively sputtered $SiO_2$ or electron beam evaporated $SiO_2$ can be used, in conjunction with high vacuum sputtering, to produce thick integral coverslips.

### 2.1.1 High Vacuum Sputtering

High vacuum sputtering is a proprietary IPC process. As such, it is Company policy to reveal only those details of the process that are pertinent to the contract objectives. Consequently, there will be no discussion of the sputtering equipment itself.

High vacuum sputtering differs from conventional glow discharge sputtering in that the material is sputtered from the target by a focused ion beam rather than by the random incidence of ions in a glow (or electron supported) discharge. Production of a focused ion beam inherently requires that the beam propagate through a low pressure region. As a consequence of this requirement, the pressure in the sputtering chamber is limited only by the gas through-put of the ion source and the speed of the pumping system. Operationally, this pressure is never higher than 1 x $10^{-4}$ torr in existing equipments. At this pressure, mean free paths of the sputtered material would be expected to be greater than ~ 50 cm, thus insuring that negligible scattering of the sputtered material occurs in its path from the target to the substrate. This is important in conjunction with the energy of the sputtered material in explaining the extremely good bonding obtained with high vacuum sputtered films. While the other aspect of sputtering at low pressure is a reduction of occluded gas in the deposited film, this factor is not particularly important in this application.

The other attributes of high vacuum sputtering are related to the use of a focused beam and its effect upon deposition rate and film bonding. Whereas the ion energy in a glow discharge is limited to 1 to 5 kev, the ion energy in a beam can be significantly increased to take advantage of the increase in sputtering yield with sputtering energy. Sputtering yield curves for most materials rise steeply from a threshold (~ 25 ev), flatten out in the region

of 35 to 60 kev, and then fall slowly. Operation in the plateau region can give a factor of ten or more increase in sputtering yield over yields obtained with glow discharge sputtering. Because the ion beam is focused, it can impinge onto the sputtering target at close to grazing incidence. This effect can produce an additional factor of 2 to 3 gain in sputtering yield over the normal incidence situation inherent in glow discharge sputtering. Thus, these two factors can increase the sputtering yield, and hence the deposition rate, by a factor of 30 or more, making high vacuum sputtering economically practical for thick (1 to 2 mil) films.

Measurements indicate that energy of the sputtered material itself runs up to ~ 100 ev, as compared to ~ 10 ev for glow discharge sputtering. Since the sputtered material is not scattered in its path from target to substrate in high vacuum sputtering, materials of this energy are incident onto the target. If indeed the increased adherence of glow discharge sputtered films, as compared to evaporated films, is due to the energy of the incident particles, up to 10 ev as compared to ~ 0.2 ev for evaporated material, the additional energy of high vacuum sputtered material would account for the extremely high film adherence that is observed. Since thermal expansion coefficients of silicon and $SiO_2$ are poorly matched, extremely good interfacial bonding is required if an integral coverslipped cell is to survive the interfacial shear stresses caused by thermal cycling.

Figure 5 is a schematic diagram of the high vacuum sputtering system used for most of the coverslip deposition work. Figure 6 is a photograph of this equipment. The system is normally operated with an argon ion beam incident onto a large fused silica target at ~ 30 deg. Both the substrate holder and target mount are water cooled. Coverslip deposition is performed at a cell temperature of 26 to 27°C. An average $SiO_2$ deposition rate is $6 \times 10^3$ Å-$hr^{-1}$. Integral $SiO_2$ coverslips over 4 mils thick have been produced on this equipment.

While high vacuum sputtering produces "good" integral coverslips, this particular piece of equipment was never designed for deposition of thick films. As a consequence, run time for a 4 mil slip is ~ 250 hr. In a period as long as this, equipment breakdown is not uncommon. This limitation plus procedural difficulties in both depositing the $CeO_2$ anti-reflection layer and cell cleaning prior to coverslip deposition have led to a number of abortive deposition runs which, in turn, have led to a small number of thick coverslip cells.

IPC, under Company funding, is presently building a production high vacuum sputtering system that is intended for solar cell coverslipping. In designing an equipment of this nature, two philosophies are possible. The first possibility is to increase beam current density while retaining the existing small beam cross section and small $SiO_2$ target. Since the number of sputtered $SiO_2$ molecules per incident ion is fixed by geometry and beam energy, this type of system would give a higher deposition rate over a small number of cells. The second approach is to increase the beam cross section and target size

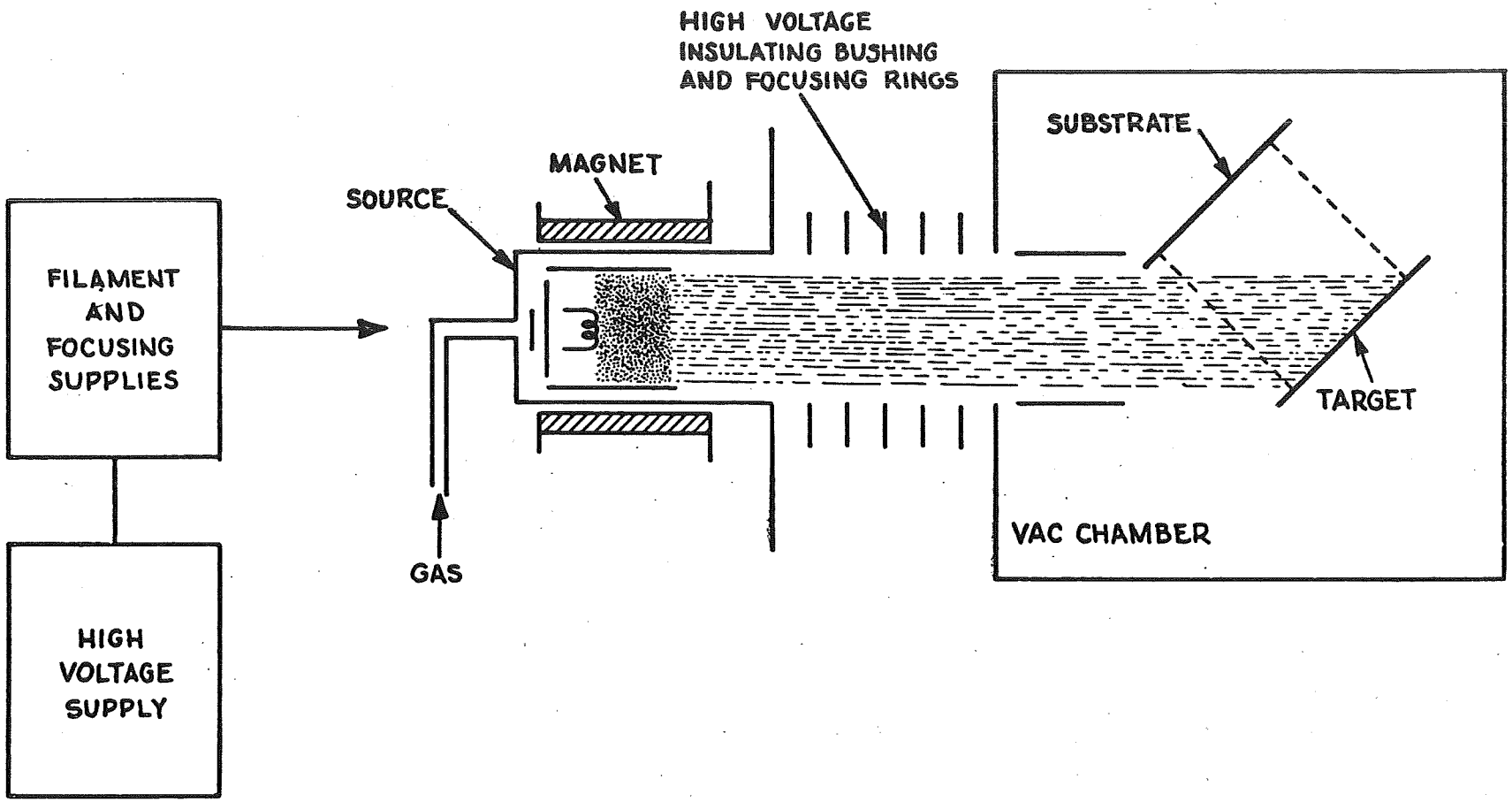


Figure 5. High Current High Vacuum Sputtering System Schematic

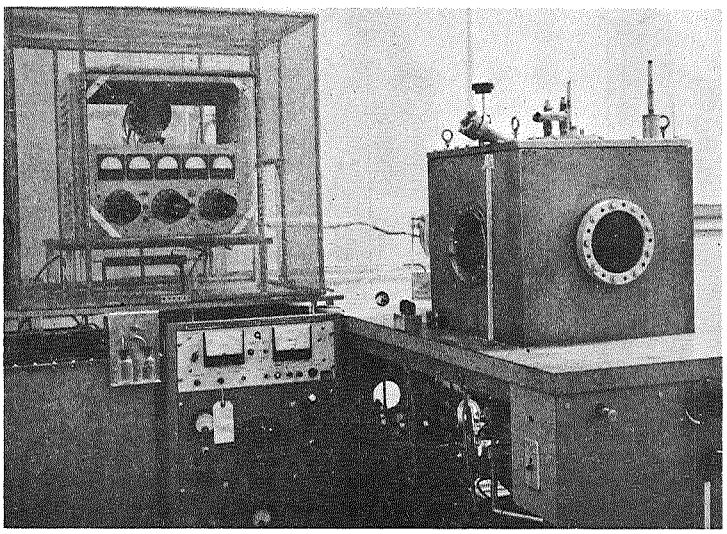

Figure 6 High Current High Vacuum Sputtering System

1-1399

while retaining the existing beam current density. This would give the existing deposition rate over a much larger number of cells. Since the latter approach is mechanically easier, it was adopted. Thus the production coverslip machine is designed to coat a very large number of cells with 1 mil of $SiO_2$ in 50 to 100 hours. (There is a good possibility that the run time will be less than 50 hr.) If the alternate techniques for depositing thick $SiO_2$ do not work out, a second production apparatus could be constructed to satisfy thick slip requirements.

### 2.1.2 Electron Beam Evaporation

The (Varian) 2 kw electron gun was finally received during the last week of September. It was set up in the throat of the small high vacuum sputtering apparatus shown in Figure 7. The gun is contained in the lower part of the chamber in the center of the photograph. The gun is shown installed in Figure 8.

Since molten $SiO_2$ does not flow under its own weight, a well focused, stable electron beam will only evaporate $SiO_2$ from a small spot in the center of the charge. This action results in formation of a conical crater in the $SiO_2$ charge and very inefficient utilization of the $SiO_2$. To overcome this problem, the electron gun permanent magnet is replaced by an air core electromagnet that is operated from a sawtooth modulated dc supply that sweeps the beam across the charge. The gun itself is operated from a constant-power dc power supply so that the power input, and hence the evaporation rate, remains constant. Unfortunately constant input power does not guarantee constant evaporation rate because of thermal non-uniformities in the charge and crucible and because of unavoidable sparking. As an alternate, IPC choose to power a permanent magnet electron gun with an unregulated dc supply. This system makes no pretense of providing a constant input power but, because of power supply fluctuations, does sweep the beam over the charge. In the long run, a servo loop rate monitoring system, with magnetic sweeping, would be required.

Initial experiments used large pieces of $SiO_2$ microscope slides placed across the top of the gun crucible. The source-to-substrate distance was ~ 10 inches. It was found, however, that power supply fluctuations were insufficient to produce enough beam sweeping to prevent cratering. To circumvent this and to provide sufficient $SiO_2$ for depositing thick coatings, a manually operated rod feed mechanism was constructed for feeding a 1/4 inch diameter $SiO_2$ rod across the top of the gun. In operation, the rod was both rocked and advanced manually in order to keep a large white-hot glob of $SiO_2$ on the end of the rod. In this manner, an experienced operator could approach constant evaporation rate. Sparking due to breakdown of $SiO_2$ deposited on the filament leads was initially quite serious. This problem was cured by encasing the leads in thick Pyrex tubing. While this solution has been very effective, "some" sparking is, reportedly, unavoidable, but, again reportedly, is not a serious problem.

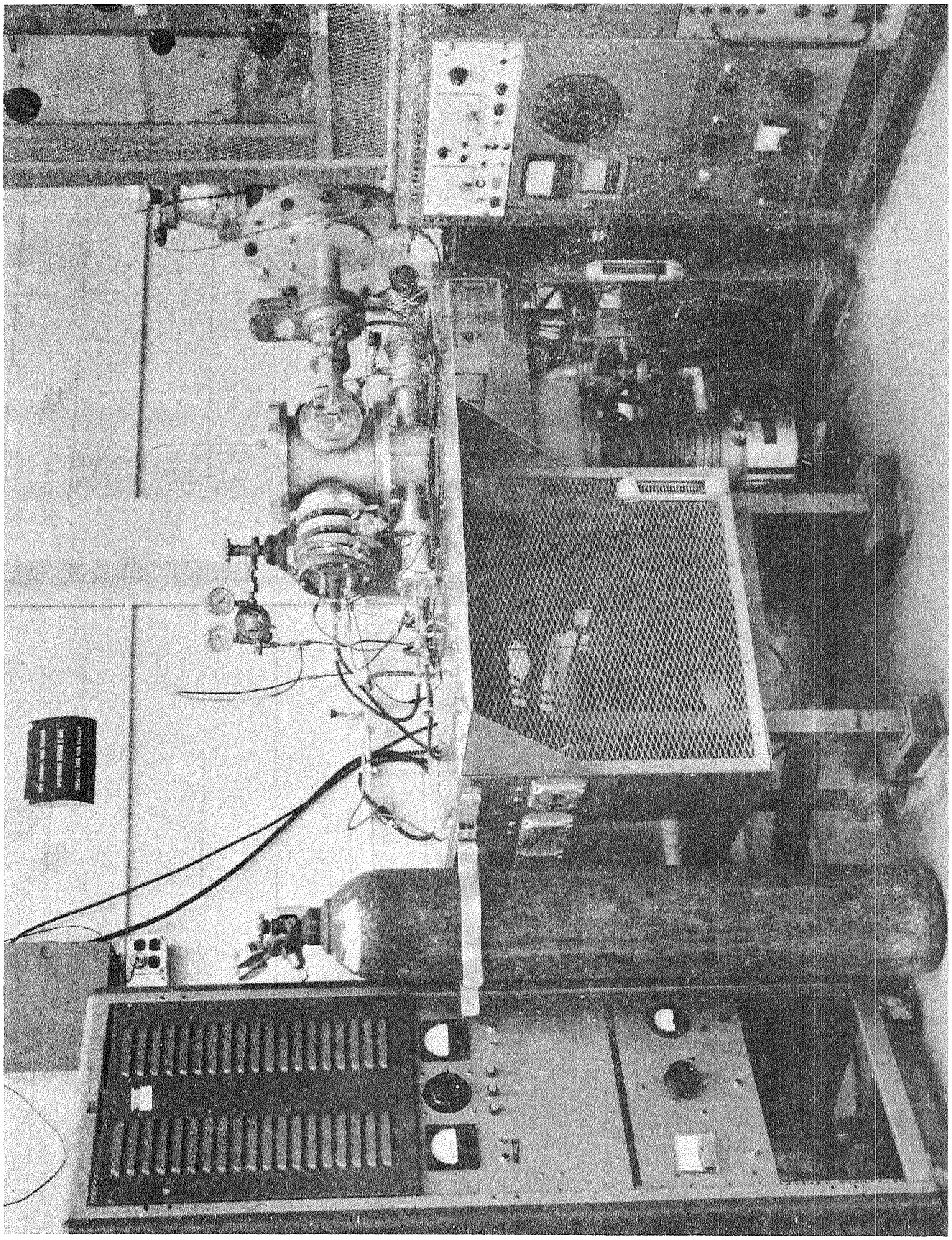

Figure 7 High Vacuum Sputtering-Electron Beam Evaporation Apparatus

2-584

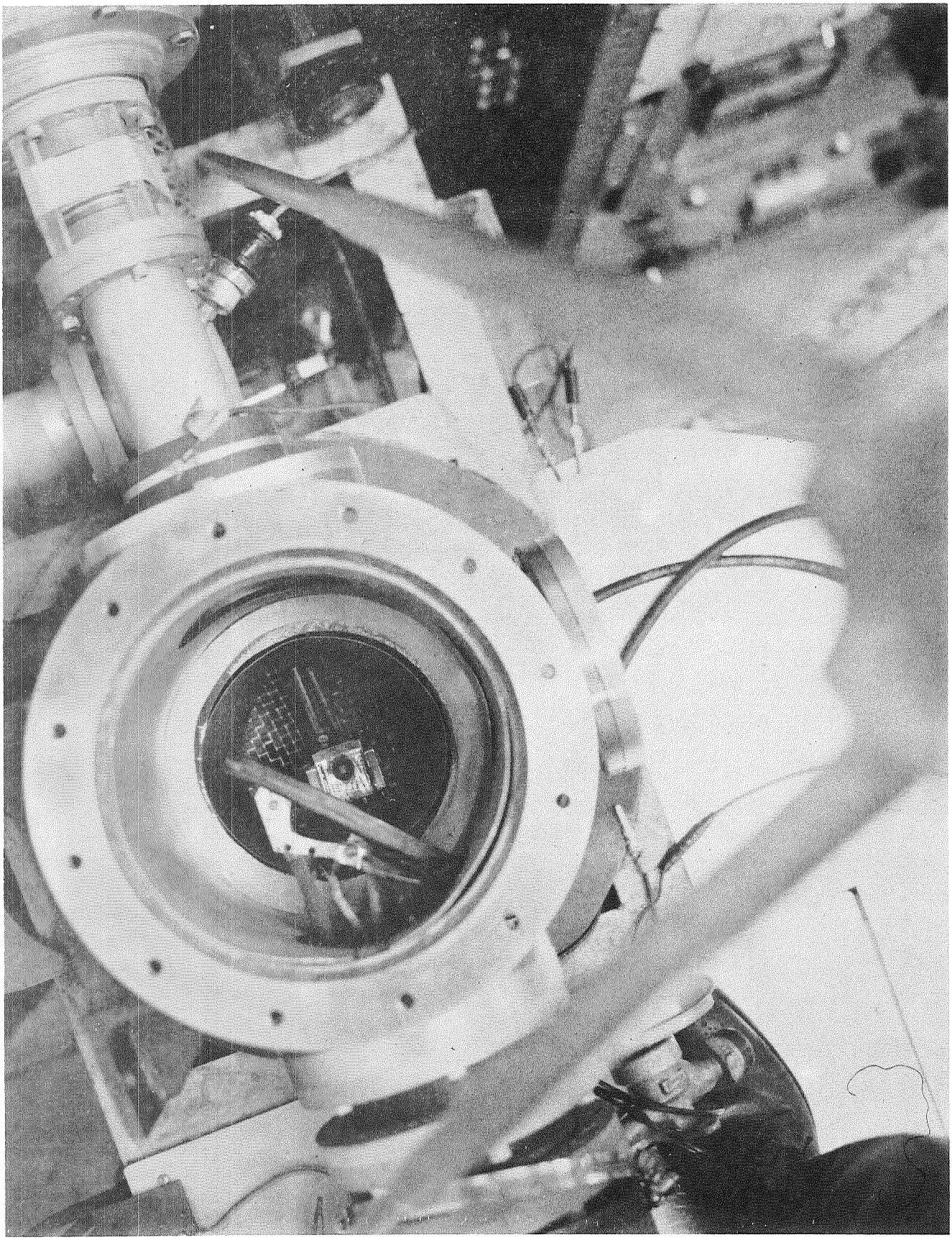

Figure 8 Installed Electron Gun

2-585

Evaporation rate, oxygen background pressure and substrate temperature are the three interconnected variables that appear to govern quality of the deposited film. For this application, the substrate temperature must, in the long run, be maintained quite near room temperature since deposition at elevated (or reduced) temperatures would result in cells that are curved at room temperature, and hence susceptible to breakage during testing and mounting. Experimentally, substrate temperature effects were found to produce the largest variations in film properties. Evaporation in a background of oxygen is necessary to prevent formation of brown SiO along with the $SiO_2$. An internal tube directing the oxygen leak at the hot source was used since this is reputedly more effective than allowing the oxygen to diffuse in the chamber. While the oxygen leak rate, and hence chamber pressure, must be proportional to deposition rate, a background oxygen pressure of $2 \times 10^{-5}$ torr was sufficient to prevent SiO formation at all available deposition rates, and was not varied.

Deposition rates were varied from 0.047 mil-min$^{-1}$ to 0.185 mil-min$^{-1}$ by control of the gun filament current. Films up to 3.5 mils thick were prepared. In general, 2 x 2 cm silicon cell blanks and $SiO_2$ microscope slides were used for substrates. Film quality was independent of substrate choice. As expected, thick evaporated $SiO_2$ films were not adherent to bare silicon but could be deposited on silicon covered with ~ 1200 A of high vacuum sputtered $SiO_2$ and on $SiO_2$ microscope slides. While most deposition was done with a substrate temperature of 30°C, substrates at 120°C and 77°K were also investigated. Films deposited on 77°K substrates spontaneously stripped when the chamber was brought to atmosphere at the end of a run. While this was probably due to differential thermal expansion problems, it may have been influenced by background gases condensing on the cold substrate at the start of the evaporation cycle. Films evaporated onto substrates at 120°C produced room temperature structures that were highly curved. Films deposited on silicon at 30°C also produced curved structures suggesting the deposited $SiO_2$ was itself strained. In general, films deposited at 120°C were slightly less adherent than films deposited at 30°C and contained a higher density of scattering centers. The latter films could usually be temperature cycled between 77 and 373°C immediately after deposition. On standing overnight, however, both cycled and uncycled thick $SiO_2$ films ofter totally crushed the silicon substrate. Fracture occurred along $\{111\}$ planes. This phenomena must be due to creep followed by fracture rather than simple fracture. Crushing did not occur with thin $SiO_2$ films and was less common with films evaporated slowly. In all cases where silicon fracture occurred, the $SiO_2$ remained bonded to the silicon. The crushing phenomena is most likely due to inherent strain in the deposited films.

From the preceding discussion, it can be seen that the bonding between evaporated $SiO_2$ and sputtered $SiO_2$ is sufficient for coverslip retention. The inherent strain in the evaporated $SiO_2$ layers must, however, be reduced. The latter can presumably be accomplished by variation of evaporation conditions although this may require evaporation onto substrates at other than room temperature. A more over-riding concern at the moment is the poor physical and optical quality of the evaporated $SiO_2$ films. On the basis of this

consideration, no acceptable evaporated films were produced. All $SiO_2$ layers were relatively soft, had low refractive index (and presumably low density), and contained a very high density of second phase optical scattering centers, These centers varied from barely resolvable to ~ 0.20 inch diameter. They were essentially circular and appeared to consist of "frothy" $SiO_2$. No variation of evaporation conditions significantly reduced their number density.

While the reason for this poor physical quality is reputedly connected with the exact evaporation conditions, thick evaporated $SiO_2$ supplied by several outside vendors has had a similar structure. The only information contrary to these observations is the claim of Temescal Metallurgical Corporation that they can evaporate thick $SiO_2$ films with good optical quality. While Temescal is the major proponent of evaporation at constant input power, it seems unlikely that this factor alone is likely to be the difference between good and bad physical structure. As previously noted, there is some doubt that constant input power actually produces a constant evaporation rate.

It is, however, observed that the density of scattering centers is very small in thin films and increases rapidly with film thickness. Moreover, some thin films supplied by outside vendors have been quite clear. It is possible that film quality is related to the geometry and mass of the $SiO_2$ charge in the electron gun. In most small electron guns, the charge is placed in an ~ 0.5 inch diameter shallow dimple in the water cooled anode. Since molten $SiO_2$ does not flow but craters in the beam, very little $SiO_2$ can be evaporated from this geometry without resorting to multiple runs. To circumvent this problem, IPC, and presumably some of the outside vendors, have resorted to feeding the gun with massive $SiO_2$ charges that are much larger than the beam dimensions. Unless it is possible to uniformly sweep the beam over the entire $SiO_2$ charge, this geometry results in molten $SiO_2$ in fairly close proximity to considerably cooler $SiO_2$. In the work done at IPC, condensation of devitrified $SiO_2$ on the cooler portions of the charge was always observed. It is likely that devitrified material is also condensed on the substrate where it may act as condensation nuclei for growth of the observed second phase scattering centers. If this overall hypothesis is correct, it may be that devitrified material is not sublimed from a fully molten $SiO_2$ charge. While this explanation fits the observations, it is presently unsubstantiated.

In view of the poor results obtained so far, all work on electron beam evaporated $SiO_2$ has been suspended pending an investigation of the Temescal claim. As an alternate to $SiO_2$, one run was made with $Al_2O_3$. The procedure used was the same as that involved in $SiO_2$ deposition, namely evaporating $Al_2O_3$ over ~ 1200 Å of $Al_2O_3$ that was high vacuum sputtered onto a silicon substrate. The evaporation charge was again a hand fed rod. Because of a limited supply of pure $Al_2O_3$ rod, only a 5 micron film could be obtained. Structurally and optically, this film was of excellent quality, free from scattering centers and well bonded to the substrate. These qualities are tempered by the fact that the film was quite thin. Unlike $SiO_2$, the viscosity of molten

$Al_2O_3$ is sufficiently low for flowing to occur. This factor makes the actual evaporation much easier, even though higher power inputs are required for $Al_2O_3$ than for $SiO_2$. A supply of pure $Al_2O_3$ rod has been ordered for a continuation of this work.

### 2.1.3 Reactive Sputtering

Because of the relatively poor results obtained with reactive sputtering, construction of the two-chamber sputtering system that was mentioned in the monthly reports has been deferred until more positive results are obtained. To date, all reactively sputtered $SiO_2$ films have contained second phase optical scattering centers. While these centers are considerably smaller than those observed in evaporated $SiO_2$ films and occur with lower frequency, they are often dark. This is thought to indicate SiO inclusions.

To review the process, reactive sputtering is a form of glow discharge sputtering wherein the inert sputtering gas is partially replaced by a gas that reacts with the sputtered material to form a compound. It is generally believed that the reaction occurs on the substrate rather than in transit or at the cathode. For $SiO_2$ deposition, a silicon target is sputtered in an argon-oxygen atmosphere. The initial reactive sputtering investigations were performed in an apparatus similar to that shown in Figure 9. The Si cathode was an ~ 2 inch diameter polycrystalline disk supported on an $SiO_2$ stand and connected to a high voltage power supply by means of a copper wire encased in glass tubing. The substrates were held in a gem holder that was suspended from a grounded metal frame. While this system produced good films, the lack of cooling allowed substrate temperatures to reach ~ 300°C.

To reduce substrate temperatures, the anode and cathode supports were inverted and the anode was water cooled. This apparatus is shown schematically in Figure 10. With this system, substrate temperatures could be limited to ~ 150°C during high rate deposition. While even this temperature is excessive, a more serious problem was the presence of scattering centers in the deposited $SiO_2$. This was thought to be due to the proximity of the $SiO_2$ cathode support to the substrate.

The next change involved a redesign of the cathode support and a change from the 2 inch diameter cathode to a 4 x 4 inch cathode that was constructed from four 1 x 4 inch bars. This arrangement is shown schematically in Figure 11. The upper $SiO_2$ plate was placed over a 3-1/2 x 3 1/2 inch piece of tantalum foil that distributed current to the individual silicon bars. This plate overlapped the edges of the cathode and contained a close fitting central hole through which the glass insulated high voltage lead was passed. The upper plate prevented sputtering from the top surface of the cathode thus reducing power dissipation at the cathode and allowing substrates to remain at ~ 25°C during deposition. The lower $SiO_2$ plate contained a 3-3/4 x 3-3/4 inch cut-out that defined the active cathode ares. The lower plate rested on 6 inch long $SiO_2$ bars that spaced the cathode from the anode. This system produced films with

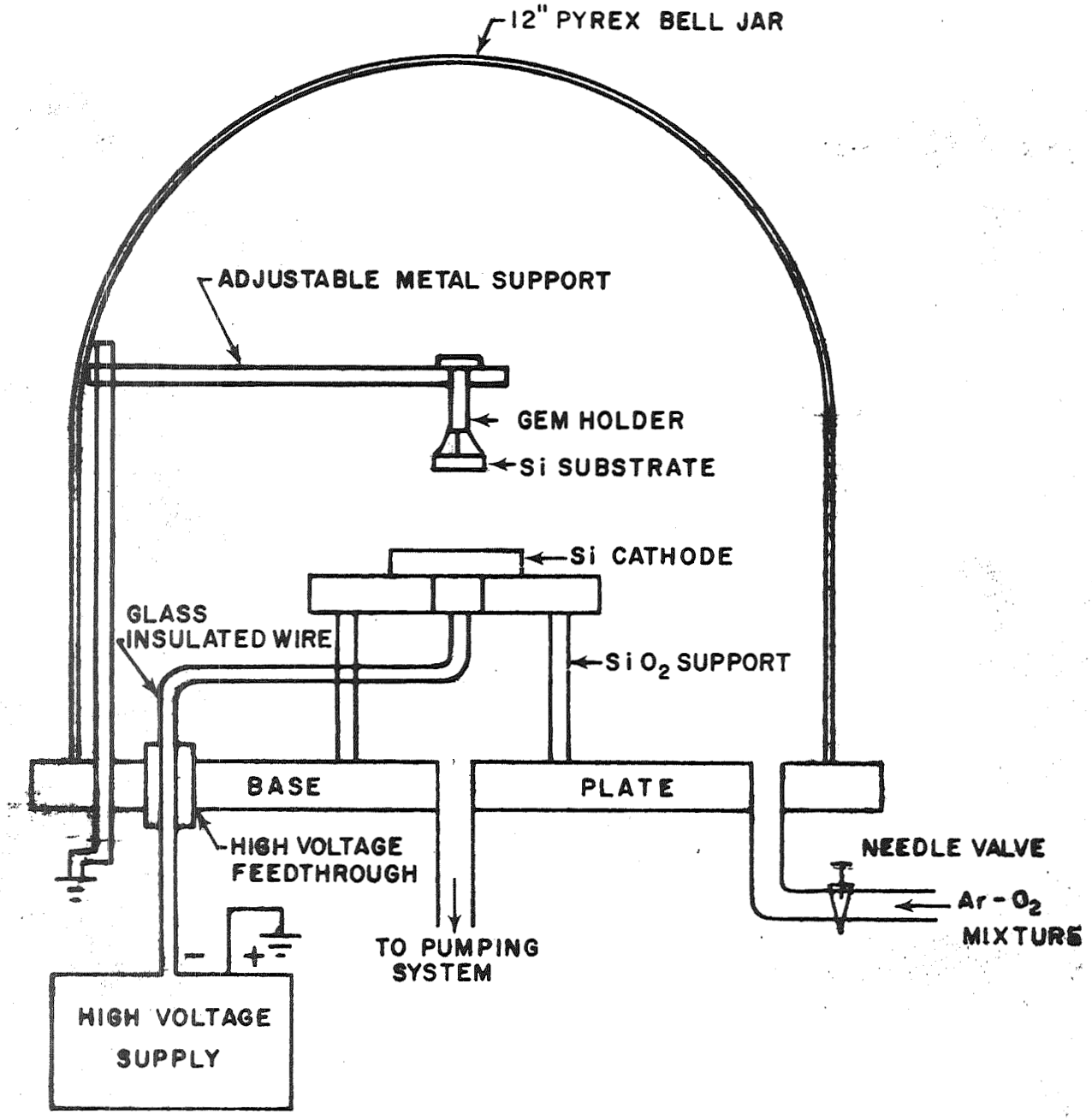


Figure 9. First Reactive Sputtering System

1-1920

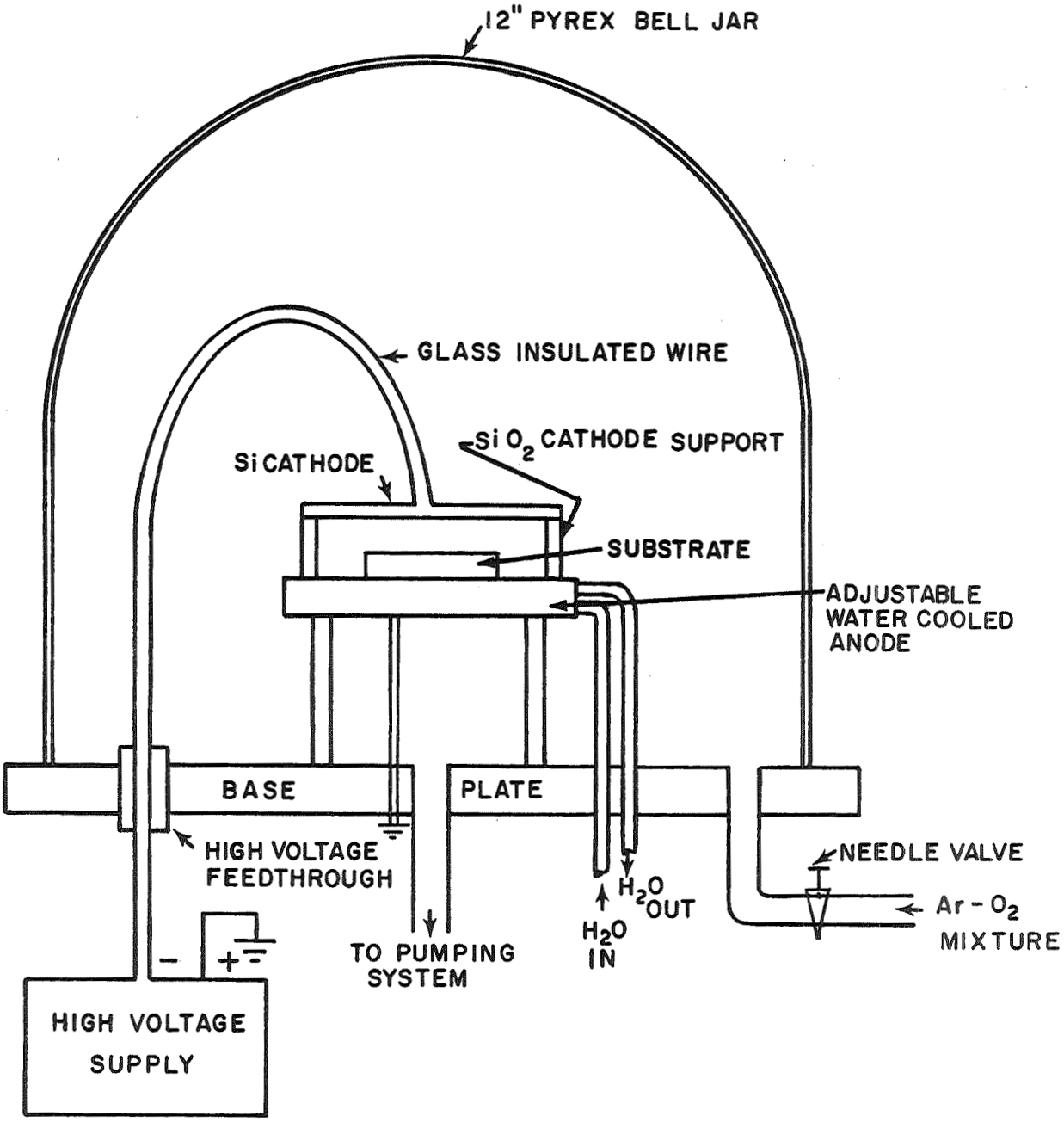


Figure 10. Second Reactive Sputtering System

1-1921

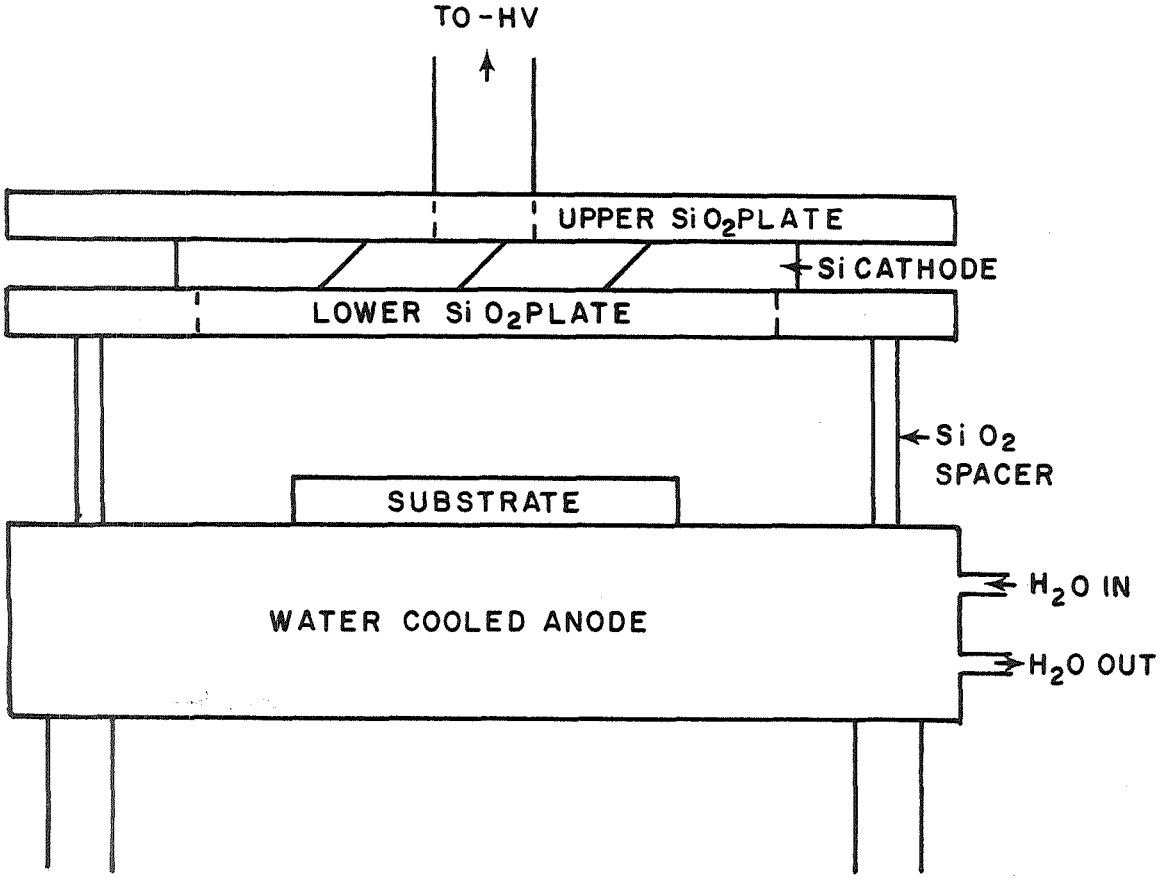


Figure 11. Third Reactive Sputtering Configuration

1-1922

an even higher density of scattering centers. Moreover, discolorations appeared on the cathode at the edges of the aperture, and to a lesser extent, at the cathode bar joints. A great deal of sparking was also observed. In extreme cases, the cathode bars were heavily eroded at the edge of the aperture. Since these defects could not be eliminated by variation of the previously optimized deposition conditions or by running the $Ar-O_2$ mixture through a dry ice-acetone trap, it was concluded, by elimination, that an interaction between the Si and $SiO_2$ support was responsible for the poor films and the cathode effects.

In the next change, the lower $SiO_2$ plate was replaced by two 1/4 inch diameter $SiO_2$ rods positioned near the ends of the cathode bars. These rods were then supported on the old 6 inch long $SiO_2$ spacer bars that were positioned about 1 inch outside the cathode. This system produced slightly better results than the previous configuration but still produced films with an unacceptable number of scattering centers. The major cathode erosion now occurred at the cathode bar joints although effects were still noticeable at the $SiO_2$ support rods. The next variation was elimination of three of the silicon cathode bars leaving a single 1 x 4 inch cathode. This configuration again produced a slight but insufficient improvement.

The next variation was a redesign of the entire apparatus such that the silicon cathode served as the top of the vacuum chamber. This system is shown schematically in Figure 12. The seal between the silicon plate and the Pyrex pipe is made with an O-ring that fits the ring groove of the pipe. The cathode is cooled by a fan mounted on a screen cage that covers the top of the apparatus. Cathode temperature is 80 to 100°C during deposition while the substrates are at ~ 25°C. Although this apparatus produced $SiO_2$ layers superior to all except the first system, the film quality was still inadequate. Sparking was always observed at the cathode perimeter. Additionally, dark deposits and cathode erosion were observed at the perimeter after a run. A radially symmetric pattern of dark deposited material could be seen on the anode. This pattern was darkest at the anode edge and faded away toward the center. Variations of sputtering voltage, gas pressure, gas mixture or anode-cathode separation did not cure these problems in films of equivalent thickness. The gas distribution ring was temporarily replaced by a single central tube aimed at the cathode center. This produced no change in film quality. Variations in anode size had a negligible effect.

It appears that the dark deposits and, perhaps, the scattering centers in the films are due to an interaction between the silicon cathode and the O-ring and Pyrex pipe. This interaction is unexpected in that one of the main considerations in adopting the geometry shown in Figure 12 was the reported observation that in sputtering with a cathode nearly the same size as the chamber, an inactive penumbra is formed at the cathode perimeter. It was expected that this penumbra would protect against interactions at the support-cathode interface. The next planned variation is to replace the silicon-O-ring-glass joint with a joint in which the O-ring is concealed from the glow.

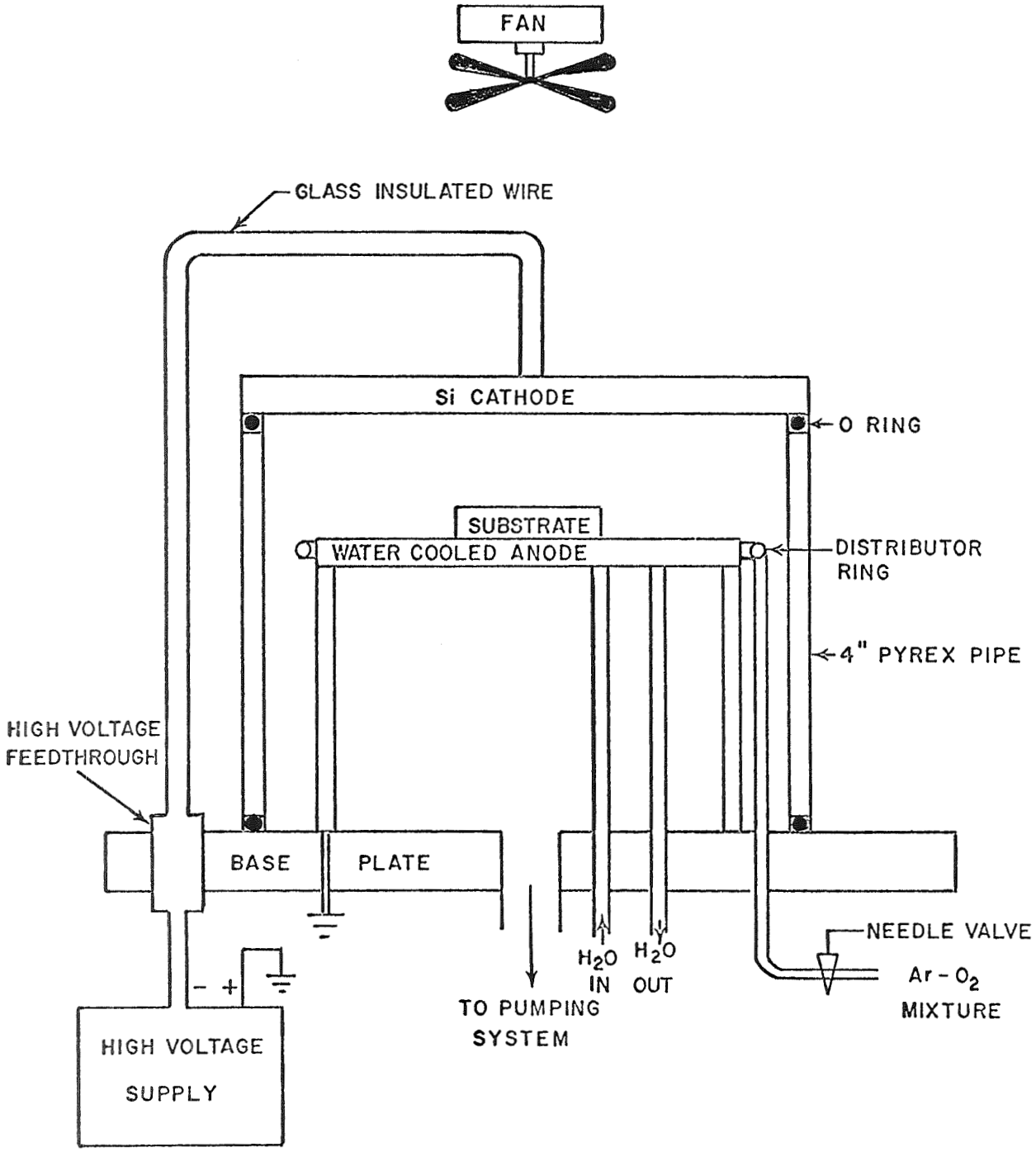


Figure 12. Sixth Reactive Sputtering System

1-1923

A short experiment on reactive sputtering of $Al_2O_3$ was run with the configuration of Figure 12. A commercial aluminum alloy cathode was used under typical $SiO_2$ deposition conditions. The resulting film was slightly dark, presumably due to large quantity of alloying material in the cathode, but was free from scattering centers. A pure aluminum cathode is being obtained for further investigation.

## 2.2 Cell Testing

### 2.2.1 Vacuum Environment

Two integral coverslipped cells were stored for 500 hours at 100 ± 1°C in a vacuum of 2 to 8 x $10^{-7}$ torr. No weight loss was observed. The data is summarized in Table 2. These test results are as expected since the integral coverslip is itself deposited in vacuum and contains no volatile materials. As the ultra violet light for the chamber had not been received, this test could not be run as a ultra violet-vacuum storage.

A second group of six cells, three with integral coverslips and three with only $CeO_2$ anti-reflection coatings is currently being run as a ultra violet-vacuum storage test at 100°C. This test is scheduled to terminate 28 January 1967.

### 2.2.2 Proton Resistance

To date, three separate proton tests have been run. In the first proton test, the unslipped contact bar was not covered during irradiation. The contact bar metallization (~ $10^4$ Å) was not sufficiently thick to prevent radiation damage in this area. As a result, the two cells in this test exhibited a reduced $V_{OC}$ and a degraded curve factor without significant $I_{SC}$ degradation. Annealing these cells at 400°C for 1 hour in argon restored the pre-irradiation values of $V_{OC}$ and CF. This data is summarized in Table 3.

The second proton test was a poorly run experiment in that the proton flux was not uniform over the cells. Thus, in any given irradiation, some cells were out of the beam while others were irradiated. Since cell positions were randomized for each radiation, no definite irradiation history could be gathered. Table 4 presents $I_{SC}$ data for these cells. All cells had 1 to 2 mil coverslips. Cells G5-26 and G7-4 had two small (~ 1 x 2 mm) notches etched through the coverslip on the 2 cm edge opposite the contact bar. $I_{SC}$ was also measured three days after the final ($10^{15}$) proton irradiation.

The rough data on the third proton test is summarized in Table 5. These cells were successively irradiated at $10^{13}$, $10^{14}$ and $10^{15}$ protons-cm$^{-2}$ at 400 kev in vacuum with a metal mask covering the unslipped contact bar. The cells were completely tested before and after each run. The solar efficiency ($\eta_s$) measurement is based on conversion of relative spectral response data to an absolute efficiency by means of a computer program. This data has

Table 2. Vacuum Storage at 100°C

| Cell Number | Weight Before Test | Weight After Test | Δ |
|---|---|---|---|
| G4-39B | 0.1761 g | 0.1761 g | 0 |
| G4-34 | 0.1770 g | 0.17695 g | +0.00005 g |

Table 3. First Proton Test

| | $V_{OC}$ (v) | | | CF | | | $I_{SC}$ (ma) | | |
|---|---|---|---|---|---|---|---|---|---|
| Cell | Start | $10^{15}$ | Heat Treated | Start | $10^{15}$ | Heat Treated | Start | $10^{15}$ | Heat Treated |
| G4-45 | 0.555 | 0.53 | 0.555 | 0.76 | 0.72 | 0.75 | 80 | 80 | 79 |
| G5-17 | 0.55 | 0.537 | 0.55 | 0.74 | 0.695 | 0.72 | 82 | 80 | 82 |

Table 4. Second Proton Test

| | $I_{SC}$ (ma) | | |
|---|---|---|---|
| Cell | No Irradiation | $10^{15}$-cm$^{-2}$ | $10^{15}$-cm$^{-2}$ + 3 Days |
| G5-26 | 85 | 85 | 86 |
| G7-4 | 84 | 80 | 83 |
| G6-16 | 83 | 84 | 84 |
| G7-25 | 83 | 82 | 84 |

Table 5. Third Proton Test

| Cell | Test | 400 kev protons-cm$^{-2}$ 0 | $10^{13}$ | $10^{14}$ | $10^{15}$ |
|---|---|---|---|---|---|
| G4-45 | $I_{SC}$ (ma) | 81.0 | 81.0 | 81.0 | 80.0 |
| | CF | 0.76 | 0.75 | 0.75 | 0.76 |
| | $\eta_S$ (%) | 9.9 | -- | -- | -- |
| | $\eta_T$ (%) | 13.6 | 13.4 | 13.4 | 13.4 |
| G5-17* | $I_{SC}$ (ma) | 82.0 | 82.0 | 82.0 | 81.0 |
| | CF | 0.75 | 0.685 | 0.70 | 0.715 |
| | $\eta_S$ (%) | 10.1 | -- | -- | -- |
| | $\eta_T$ (%) | 13.5 | 12.3 | 12.6 | 12.7 |
| G4-44 | $I_{SC}$ (ma) | 82.0 | 82.0 | 82.0 | 81.0 |
| | CF | 0.755 | 0.735 | 0.735 | 0.74 |
| | $\eta_S$ (%) | 10.5 | -- | -- | -- |
| | $\eta_T$ (%) | 14.0 | 13.5 | 13.5 | 13.5 |
| G5-8B | $I_{SC}$ (ma) | 80.0 | 81.0 | 81.0 | 81.0 |
| | CF | 0.73 | 0.71 | 0.71 | 0.70 |
| | $\eta_S$(%) | 10.1 | -- | -- | -- |
| | $\eta_T$ (%) | 13.0 | 12.9 | 12.8 | 12.6 |

* This cell had a growing coverslip blemish.

not been reduced yet. Tungsten efficiency ($\eta_T$) is obtained from comparison to the output of a "standard" cell illuminated at 140 mw-cm$^{-2}$ by a tungsten lamp. $I_{SC}$ and curve factor (CF) are obtained from tungsten I-V characteristics. The overall accuracy of the testing procedures is estimated to be ± 3%.

All cells in this test had 1 to 1.2 mil coverslips assuring that all protons were stopped in the coverslip. Cells G4-45 and G5-17 had been irradiated in the first proton test and subsequently annealed at 400°C for 1 hour. A "bubble" developed in the coverslip of G5-17 during the annealing step. This bubble became noticeably larger during irradiation in the third test and could certainly account for the degradation that was observed. Cells G4-44 and G4-45 had notches similar to those described in the second proton test. Irradiation of these small cell areas had no apparent effect on cell response.

## 3. FUTURE PLANS

Again the date for choice between electron beam evaporation and reactive sputtering as a means of building up coverslip thickness must be moved back because of poor results with both systems. This slippage should not effect the final schedule. For the next three months, work on evaporated $SiO_2$ will be discontinued pending an evaluation of the Temescal claim. Work on evaporated $Al_2O_3$ will continue when the $Al_2O_3$ rods are received. Reactive sputtering of $SiO_2$ will be continued at a reduced level. Reactive sputtering of $Al_2O_3$ will be deferred until an optimum geometry for the reactive sputtering apparatus can be established. Cell testing will be conducted as scheduled.

## 4. REFERENCES


(1) "Calculations of Energy Loss, Range, Path Length, Straggling, Multiple Scattering and the Probability of Elastic Nuclear Collisions for 0.1 to 1000 Mev Protons", AFWL-TR-65-150 (1966) (J. Janni).

(2) "Range-Energy Relations for Protons and Electrons in Al, Si and $SiO_2$", NRL Report 5828 (1962) (V. J. Linnenbom).

(3) "Radiation Damage in Solids", D. S. Billington and J. H. Crawford, Princeton University Press, Princeton (1961) (p. 249 ff).

(4) "Radiation Damage in Solids, Course 18", Proceedings of the International School of Physics, D. S. Billington (Editor), Academic Press, New York (1962) (p. 518 ff).

(5) "Radiation Damage in Solids, Course 18", Proceedings of the International School of Physics, D. S. Billington and J. H. Crawford, Academic Press, New York (1962) (p. 281-3).

(6) "Radiation Damage in Solids, Course 18", Proceedings of the International School of Physics, D. S. Billington and J. H. Crawford, Academic Press, New York (1962) (p. 280-1).

DISTRIBUTION LIST

| Addressee | Copies |
|---|---|
| NASA-Goddard Space Flight Center<br>Greenbelt, Maryland 20771<br>Attention: | |
| Office of the Director - Code 100 | 1 |
| Office of the Assistant Director for Administration and Technical Services - Code 200 | 3 |
| Office of the Assistant Director for Projects - Code 400 | 1 |
| Office of the Assistant Director for Systems Reliability - Code 300 | 1 |
| Office of the Assistant Director for Tracking and Data Systems - Code 500 | 1 |
| Office of the Assistant Director for Space Sciences - Code 600 | 1 |
| Office of the Assistant Director for Technology - Code 700 | 1 |
| GSFC Library - Code 252 | 2 |
| Contracting Officer - Code 247 | 1 |
| Technical Information Division - Code 250 | 4 |
| Technical Representative - Code 716 | 25 |
| NASA Headquarters<br>FOB 10B<br>Washington, D.C. 20546<br>Attn: Arvin Smith, Code RNW | 1 |
| Anderson, Donald<br>NASA/Ames Research Center<br>Moffett Field, California | 1 |
| Bachner, Robert L.<br>Solar Systems, Inc.<br>8241 N. Kimball Avenue<br>Skokie, Illinois 60078 | 1 |

| Addressee | Copies |
|---|---|
| Baicker, J. A.<br>Princeton Research and Development Company<br>Box 641<br>Princeton, New Jersey | 1 |
| Barkley, Dwight W.<br>Liberty Mirror, L. O. F.<br>Brackenridge, Pennsylvania 15014 | 1 |
| Brancato, E. L.<br>N. R. L.<br>Washington, D. C. | 1 |
| Chamberlin, R. R.<br>National Cash Register Company<br>Main and K Streets<br>Dayton, Ohio | 1 |
| Cherry, William R.<br>NASA/Goddard Space Flight Center<br>Greenbelt, Maryland 20771 | 1 |
| Cole, Robert L.<br>Texas Instruments<br>Dallas, Texas | 1 |
| Cusano, Dominic A.<br>General Electric, R&D Center<br>P. O. Box 1088<br>Schenectady, New York | 1 |
| Dawson, John R.<br>NASA/Langley Research Center<br>Langley Station<br>Mail Stop 188-B<br>Hampton, Virginia 23365 | 1 |
| Downing, R. G.<br>TRW Systems<br>1 Space Park<br>Redondo Beach, California | 1 |
| Fang, P. H. (Dr.)<br>NASA/Goddard Space Flight Center<br>Greenbelt, Maryland 20771 | 1 |

| Addressee | Copies |
|---|---|
| Ferguson, George D. (Jr.)<br>General Electric<br>Carroll Avenue<br>Lynchburg, Virginia | 1 |
| Finger, Harold B<br>NASA Headquarters<br>Washington, D. C. 20546 | 1 |
| Fischell, Robert<br>JHU/Applied Physics Laboratory<br>Silver Spring, Maryland | 1 |
| Hamilton, Robert C.<br>Institute for Defense Analyses<br>400 Army-Navy Drive<br>Arlington, Virginia 22202 | 1 |
| Hawkins, Kenneth D.<br>Ryan Aeronautical Company<br>Lindberg Field<br>San Diego, California 92112 | 1 |
| Haynes, Gilbert A.<br>NASA/Langley Research Center<br>Langley Station<br>Hampton, Virginia 23365 | 1 |
| Holloway, H.<br>Philco Research Laboratory<br>Blue Bell, Pennsylvania | 1 |
| Hood, John<br>Dow Corning Corporation<br>Hemlock, Michigan 48626 | 1 |
| Iles, Peter A.<br>Hoffman Electronics Corporation<br>4501 Arden Drive<br>El Monte, California | 1 |
| Jilg, Eugene T.<br>Communications Satellite Corporation<br>2100 L Street, N. W.<br>Washington, D. C. 20037 | 1 |

| Addressee | Copies |
|---|---|
| Johnson, Carl E.<br>Bellcomm, Inc.<br>1100 17th Street, N. W.<br>Washington, D. C. | 1 |
| Julius, Richard F.<br>Keltec Industries, Inc.<br>5901 Edsall Road<br>Alexandria, Virginia 22314 | 1 |
| Kaye, S.<br>Electro-Optical Systems Inc.<br>300 No. Halstead Street<br>Pasadena, California | 1 |
| King, W. J. (Dr.)<br>Ion Physics Corporation<br>Burlington, Massachusetts 01803 | 1 |
| Kittl, Emil<br>U. S. Army Electronics Command<br>Attn: AMSEL-KL-PA<br>Fort Monmouth, New Jersey CC-07703 | 1 |
| Kling, Harry P.<br>Hittman Associates<br>Beltimore, Maryland | 1 |
| Loferski, Joseph J. (Dr.)<br>Brown University<br>Providence, Rhode Island | 1 |
| Marks, Burton S.<br>Lockheed Missile and Space Company<br>Palo Alto, California | 1 |
| Massie, Lowell D.<br>AF Aero Propulsion Laboratory<br>APIP-2<br>Wright-Patterson Air Force Base, Ohio | 1 |
| Mlavsky, A. I. (Dr.)<br>Tyco Laboratories, Inc.<br>Bear Hill<br>Waltham, Massachusetts 02154 | 1 |

| Addressee | Copies |
|---|---|
| Mott, James L.<br>Fairchild Hiller Corporation<br>Rockville, Maryland | 1 |
| Oman, Henry<br>Boeing Company<br>Seattle, Washington 98166 | 1 |
| Pearson, Gerald L.<br>Stanford University<br>Stanford, California | 1 |
| Potter, Andrew<br>NASA/Lewis Research Center<br>21000 Brookpark Road<br>Cleveland, Ohio 44135 | 1 |
| Plauche, Fulton M.<br>NASA/Manned Space Flight Center<br>EP-5<br>Houston, Texas 77058 | 1 |
| Ralph, E. L.<br>Heliotek<br>12500 Gladstone Avenue<br>Sylmar, California | 1 |
| Rappaport, Paul<br>RCA Laboratories<br>Princeton, New Jersey | 1 |
| Ray, Kenneth A.<br>Hughes Aircraft Company<br>El Segundo, California | 1 |
| Reynard, Duncan L.<br>Philco WOL<br>Palo Alto, California | 1 |
| Riel, Robert K.<br>Westinghouse Electric Corporation<br>Semiconductor Division<br>Youngwood, Pennsylvania 15697 | 1 |

| Addressee | Copies |
|---|---|
| Ritchie, Donald W.<br>Jet Propulsion Laboratory<br>Pasadena, California | 1 |
| Schach, Milton<br>NASA/Goddard Space Flight Center<br>Greenbelt, Maryland 20771 | 1 |
| Schaefer, James C.<br>Harshaw Chemical Company<br>1945 E. 97th Street<br>Cleveland, Ohio | 1 |
| Schlotterbeck, R. S.<br>General Electric Company<br>Lynchburg, Virginia | 1 |
| Schwarz, F. C.<br>NASA/ERC<br>575 Technology Square<br>Cambridge, Massachusetts 02139 | 1 |
| Shirland, F. A.<br>Clevite Corporation<br>540 E. 105th Street<br>Cleveland, Ohio 44108 | 1 |
| Slifer, Luther W. (Jr.)<br>NASA/Goddard Space Flight Center<br>Greenbelt, Maryland | 1 |
| Timberlake, Allen B.<br>Battelle Memorial Institute<br>505 King Avenue<br>Columbus, Ohio 43201 | 1 |
| Waddel, Ramond C. (Dr.)<br>NASA/Goddard Space Flight Center<br>Greenbelt, Maryland 20771 | 1 |
| Winkler, Seymour H.<br>RCA/AED<br>P. O. Box 800<br>Princeton, New Jersey 08540 | 1 |

| Addressee | Copies |
|---|---|
| Wise, Joseph F.<br>USAF-APL APIP-2<br>Wright-Patterson Air Force Base<br>Dayton, Ohio | 1 |
| Yannoni, Nicholas F.<br>AF Cambridge Research Laboratories<br>L. G. Hanscom Field<br>Bedford, Massachusetts 01731 | 1 |
| Wolf, Martin<br>RCA/AED<br>Princeton, New Jersey | 1 |
| Marinozzi, D.<br>Optical Coating Laboratories<br>Santa Rosa, California | 1 |
| Starkey, Gerald E. (Major)<br>Headquarters USAF<br>AFRSTD Pentagon<br>Washington, D. C. | 1 |
| Werth, John J.<br>General Motors<br>Defense Research Laboratories<br>6767 Hollister Avenue<br>Goleta, California | 1 |